Desalination and Water Treatment
www.deswater.com

doi:10.5004/dwt.2019.23501

141 (2019) 342–355
February

Chitosan-containing organoclays: Structural characterization and retention/removal of methylene blue

Sarra Kabbadj, Mohamed Hajjaji*, Abdelhakim Alagui

Laboratoire de Physico-chimie des Matériaux et Environnement, Faculté des Sciences Semlalia, Université Cadi Ayyad, B.P. 2390, Av. Pce My Abdellah, 40001, Marrakech, Morocco, email: sarra.kabbaj@gmail.com (S. Kabbadj), Fax +212 5 24 43 74 08, email: hajjaji@uca.ma (M. Hajjaji), alagui@ucam.ac.ma (A. Alagui)

Received 14 August 2018 ; Accepted 25 November 2018

ABSTRACT

Organoclays, composed of chitosan and stevensite-rich clay (RH) or kaolinitic-illitic clay (BN2), were structurally characterized, and their adsorption abilities for methylene blue (MB) were investigated by XRD, FT-IR, UV-vis spectroscopy and SEM. The effects of pH, ionic strength (I) and temperature (T) on MB desorption were evaluated by using the response surface methodology (RSM). The results showed that the chitosan was placed within interlamellar spaces of swelling clay minerals, and around clay and ancillary particles, and the kinetics of MB adsorption was generally controlled by film-diffusion. MB adsorption occurred spontaneously ($-41 < \Delta G° < -32$ kJ/mol), and the Langmuir maximum adsorption capacity of RH-based composite (138 mg/g at 298 K) was about three times higher than that of BN2-based composites. MB species were adsorbed by cation exchange, and they were located at surfaces of composite particles as MB^+, $(MB^+)_2$ and $(MB^+)_3$. Also, they were attached to surficial chitosan mainly by means of amino-groups. The results of RSM showed that the increase of one among the above factors had a negative impact on MB desorption, and the weights of the effects of the factors followed the order pH > T > I.

Keywords: Organoclays; Chitosan; Methylene blue; Adsorption; RSM; Desorption

1. Introduction

Because of their nano-sized particles, specific structures and the presence of diverse functional groups, organoclays are considered as potential adsorbents for the uptake of various hazardous chemical species [1]. Clay minerals, especially those belonging to the group of smectites, such as montmorillonite and stevensite, are suitable starting materials for organoclays preparation [2]. The use of these minerals is motivated by the high ratio surface to volume of their particles and cation exchange capacity, and by their expandable interlayer space. Chitosan, which is a chitin-derivative amino-polysaccharide biopolymer, is considered as an appropriate component for the elaboration of organoclays [3]. The chemical reactivity of chitosan is essentially linked to its amino-groups and hydroxyls.

Organoclays, composed of smectite clay minerals and chitosan, have been the subject of studies related to their structures [4–6]. The results showed that the chitosan chains could be inserted within interlayer spaces, and consequently different structures of composites (intercalated, exfoliated, flocculated) could be formed, depending on the layers of chitosan within the interlayer spaces. The formation of chitosan-montmorillonite composites, for instance, was essentially attributed to the attractive forces between the negative charged sites of montmorillonite and protonated amino-groups of chitosan, and also to the development of hydrogen bonds between hydroxyls of montmorillonite and amino-groups.

Methylene blue is a cationic dye, found in effluents of dyeing factories and dye manufacturing plants. MB contaminated waters can have various detrimental effects on human health [7]. According to a clinical survey [8], the-

*Corresponding author.

harmful effects of MB are manifested as the dose exceeds 2 µg/g. The removal of MB from highly concentrated aqueous solutions can be successfully realized by chemical precipitation. In contrast, adsorption seemed to be an efficient and economical technique for the uptake of MB from diluted solutions [7].

The retention of methylene blue by composites made from chitosan (pristine or chemically modified) and clays was the object of studies [3,9]. These studies focused mainly on the determination of the maximum adsorption capacity of MB, and modeling of kinetics and isotherms data. Nonetheless, the characteristics of the clays used were often ignored, and little attention was paid to the adsorption mechanisms of MB-derivative species as well as to the regeneration of the dye.

The aim of this study was to: i) Carry out a structural characterisation of binary organoclays composed of stevensite-rich clay(RH), kaolinitic-illitic clay (BN2) and chitosan, which was prepared from shell shrimps. ii) Determine the adsorption mechanisms of methylene blue on the organoclays prepared. iii) Follow the desorption efficiency of MB in different aqueous solutions. This study was realized with the help of the response surface methodology.

2. Materials and experimental procedures

2.1. Materials

2.2. Clays

The clays used, labeled RH and BN2, originated from Fès-Boulmane and Tétouan-Hoceima regions (Morocco) respectively. Stevensite was the main clay mineral found in RH. BN2 was composed of an assemblage of clay minerals: illite, kaolinite and a smectite clay mineral. The ancillary minerals in both clays are indicated in Fig. 1a. The cation exchange capacities (CEC) of RH and BN2 were determined to be 0.8 and 0.3 meq/g respectively.

To be used, the clays were decarbonated and saturated with sodium. Then, they were stored in a drying oven at 105 °C.

2.1.2. Chitosan

Chitosan was prepared from shells of shrimps following the experimental procedures described by Ba et al. [10]. Typical X-ray diffraction pattern of the chitosan prepared is shown in Fig. 1b. The molecular weight and the deacetylation degree of chitosan were estimated to be 53819 g/mol and 90% respectively. The methods followed for the determination of the latter characteristics were similar to those given elsewhere [11–13].

2.1.3. Composites chitosan-clays

For RH- and BN2-based composites preparation, a portion of sodium-saturated clay was introduced into 100 mL of a solution of acetic acid (1% v/v) containing a weighted amount of chitosan. The optimum amount of chitosan used (10 wt%) corresponded to the maximum uptake of MB by the composites (Fig. 2). By using such amount of chitosan, the loadings of RH and BN2 were determined to be 77 and 200% CEC respectively. For the preparation of the studied composites containing 10 wt% chitosan, a dispersion (100 mL) composed of Na-saturated clay (1.8 g) and chitosan (0.2 g) was stirred for 3 h at room temperature, and centrifugated at 2000 rpm. The residue obtained was washed with distilled water until the pH value of the washing solution was of 7. The organoclays obtained were oven-dried, ground (< 80 µm) and stored in the oven at 50°C.

2.2. Experimental procedures

2.2.1. Kinetics

For the study of the kinetics of MB adsorption on composites, a dispersion (150 mL), composed of the organoclay (0.075 g) and MB (0.1 mmol/L), was prepared, and continually stirred by using a magnetic agitator. The pH of the dispersion was naturally fixed at 8.5. It should be noted that, in the latter operating conditions, the amounts of MB

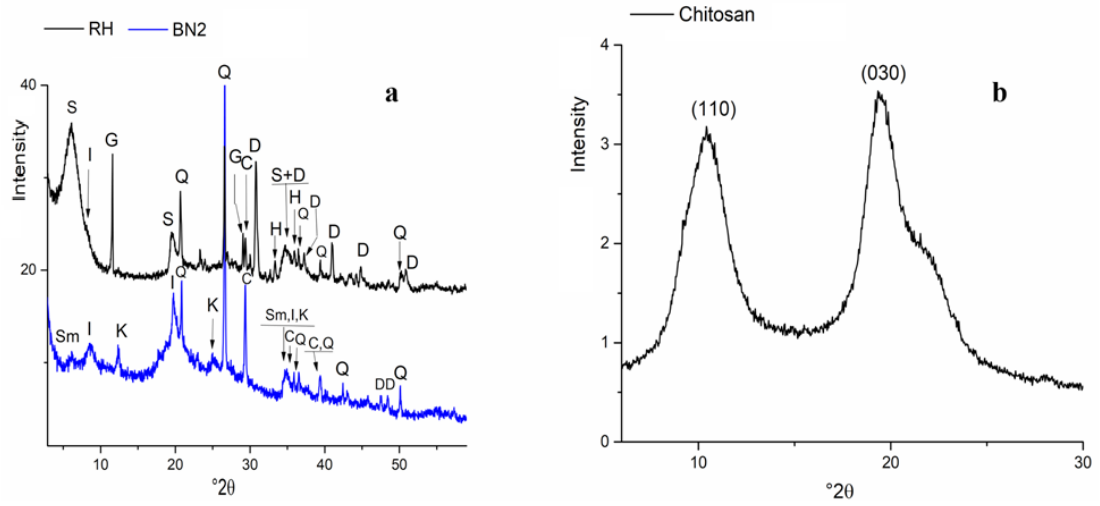

Fig. 1. X-ray diffraction patterns of the materials used. (a): raw clays; (b): chitosan. S: stevensite; I: illite; K: kaolinite; Sm: smectite clay mineral; G: gypsum; Q: quartz; C: calcite; D: dolomite; H: hematite.

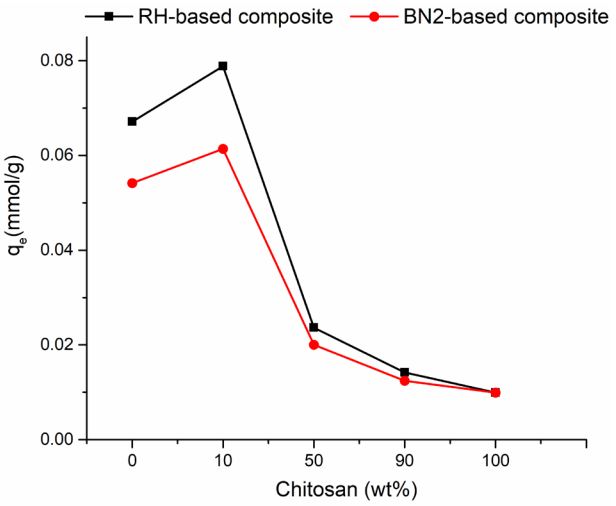

Fig. 2. Variations of the maximum adsorption capacities of RH-chitosan and BN2-chitosan composites versus amount of chitosan.

retained were very close to the maximum ones (Fig. 3). The operating temperatures varied in the range of 15–45°C. The instantaneous concentration of MB in the dispersion was measured by using a UV-visible spectrophotometer JP Selecta, operating at 664 nm, and the curve expressing the Beer-Lambert law. The measurements were made on the supernatants of samples taken from the dispersion at different times. The mathematical relation used for the determination of the instantaneous amount of MB retained (q_t; mmol/g) was as follows:

$$q_t = \frac{(C_o - C_t)\cdot V}{m} \tag{1}$$

C_o and C_t (mmol/L) are the initial and the instantaneous concentrations of MB in solution; m: mass of composite (g); V: volume of solution (L).

The kinetics data were fitted to the non-linear equations of the pseudo-first and pseudo-second order kinetics models given in Table 1. The fitting was realized with the Addinsoft XLSTAT Microsoft software, and its suitability was evaluated on the basis of the values of the correlation coefficient (R^2) and the root mean square of the error (RMSE) (Table 1).

The rate-limiting step was evaluated by using the equation derived from the model of Boyd [14]:

$$Bt = \left[\sqrt{\pi} - \left(\pi - \frac{\pi^2 F(t)}{3}\right)^{1/2}\right]^2 \tag{2}$$

(t: time; B: Boyd's number; $F(t) = q_t/q_e$, q_t and q_e were calculated according to Eq. (1) ; $F(t) \leq 0.85$).

2.2.2. Isotherms measurement

For the plot of the adsorption isotherms, solutions (25 mL) containing composite (0.5 g/L) and MB (0.01–0.1 mmol/L) were prepared, and maintained at 15, 25 or 45°C. The pH of the solutions was maintained at 8.5. After 120 min of contact, the supernatant was isolated by centrifugation at 2000 rpm, and the MB concentration was measured as previously mentioned.

The experimental isotherms were analyzed with the models of Langmuir [15], Freundlich[16], and Temkin and Pyshev [17] given in Table 1. The best fitting model was assessed by comparing the values of R^2 and RMSE.

2.2.3. Dye regeneration

The release of MB was followed in different aqueous solutions with different ionic strength (I), temperature (T) and pH. To reduce the number of experiments, the response surface methodology (RSM) was used, and the following quadratic model was adopted:

$$Y = b_o + \sum_{i=1}^{k} b_i X_i + \sum_{i=1}^{k} b_{ii} X_{ii}^2 + \sum_{1\leq i\leq j}^{k} b_{ij} X_i X_j \tag{3}$$

Y is the studied property taken here as the desorption efficiency:

$$D = 100 C_r \cdot V/m \cdot q_m \tag{4}$$

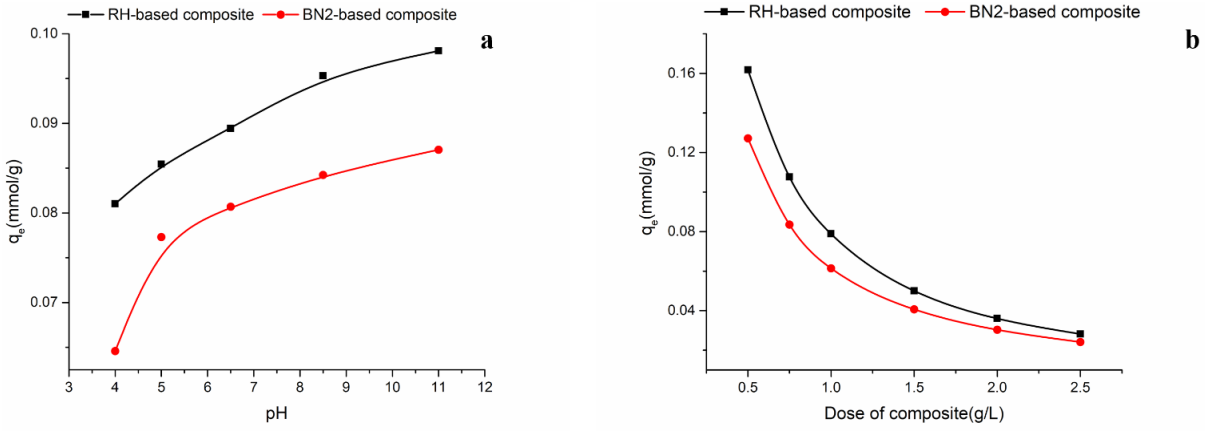

Fig. 3. Changes of the maximum adsorption capacities of the composites studied as a function of pH (a) and dose of composite (b).

Table 1
Mathematical expressions of the models and the statistical coefficients used

Kinetics and isotherms models		
Pseudo- first order kinetic equation	$q_t = q_e\left(1 - e^{-k_1 t}\right)$	k_1: pseudo first-order rate constant (min^{-1}) q_e: amount of MB retained at equilibrium (mmol/g)
Pseudo- second order kinetic equation	$q_t = \frac{k_2 q_e^2 t}{1 + k_2 q_e t}$	k_2: pseudo second-order rate constant ($g{\cdot}mmol^{-1}{\cdot}min^{-1}$)
Langmuir isotherm	$q_e = \frac{K_L C_e q_m}{\left(1 + K_L C_e\right)}$	K_L: constant of Langmuir q_m: maximum uptake of MB (mmol/g) C_e: concentration of MB at equilibrium (mmol/L)
Freundlich isotherm	$q_e = K_F\left(C_e\right)^{1/n}$	K_F: constant of Freundlich ($mmol/g{\cdot}(L/mmol)^{1/n}$)
Temkin isotherm	$q_e = \frac{RT}{b} Ln\left(K_T C_e\right)$	K_T: constant of Temkin (L/mmol) R: gas constant ($8.31\ J{\cdot}K^{-1}mol^{-1}$) T: temperature (K) b: constant ($10^3 J{\cdot}g{\cdot}mol^{-2}$)
Equations of statistical coefficients		
$R^2 = 1 - \frac{\Sigma\left(q_{exp} - q_{cal}\right)^2}{\Sigma\left(q_{exp} - \bar{q}_{exp}\right)^2}$	$RMSE = \sqrt{\frac{\Sigma\left(q_{exp} - q_{cal}\right)^2}{n}}$	q_{exp} and q_{cal}: experimental and calculated retained amounts of MB $\bar{q}_{exp}$: average of the values of q_{exp} n: Number of experiments realized

C_r: concentration of the released dye (mg/L); q_m: maximum amount of MB retained (mg/g); m: mass of the organoclay used (g); V: volume of solution (L). b_o, b_i, b_{ii} and b_{ij} are constant. b_i represents the weight of the factor "i" (ionic strength, temperature or pH). b_{ii} is considered as a curve shape parameter. b_{ij} expresses the weight of the effect of the interaction between factors "i" and "j". k is the number of the experimental factors studied. In the present study, $k = 3$. X_i is the coded variable related to the real value (v_i) of the factor "i".

$$X_i = \frac{v_i - v_i^o}{\Delta v_i}\beta \quad (5)$$

v_i^o is the central value of the investigated domain ($0 \le I \le 0.1$ M; $20 \le T \le 60$°C; $4 \le pH \le 9$); Δv_i is the step variation ($\Delta v_I = 0.05$ M ; $\Delta v_T = 20$°C; $\Delta v_{pH} = 2.5$). β is the major coded limit value. The coded variables associated to I, T and pH were denoted X_1, X_2 and X_3 respectively.

The constants of the model were determined by adopting the matrix of Doehlert [18] and by using the method of least-square regression [19]. According to the RSM, the number of experiments (n) needed in this study was 15. This was determined from the relation: $n = k^2 + k + C$; k kept the same meaning, C = 3 (number of the centers of the investigated domains). The planned experiments and the measured desorption efficiencies, which were used for the calculation of the above coefficients, are reported in Table 2.

2.2.4. Investigation techniques

The X-ray diffraction (XRD) analysis was carried out on powder samples by using a Philips X'Pert MPD diffractometer operating with a copper anode ($\lambda_{K\alpha}$ = 1.5418 Å). The Fourier transform infrared (FT-IR) analysis was performed on shaped thin discs composed of 1 mg of organoclay and 99 mg of KBr. The FT-IR spectra were recorded in the range of 4000–400 cm^{-1} with a Perkin Elmer 1725 spectrophotometer. The deconvolution of IR bands was realized with the PeakFit v4.12 software (Peak type: Gaussian shape), and the best fit was evaluated on the basis of the values of the correlation coefficient (R^2), standard error (SE) and F-statistic. The examination of the microstructure of carbon-coated particles of the organoclays was realized with a JEOL JMS 5500 scanning electron microscope (SEM), equipped with an EDAX Falcon spectrophotometer.

3. Results and discussion

3.1. Structural characterization of the adsorbents

Considering the X-ray diffractograms shown in Figs. 1a and 4, the distance of the basal X-ray reflexions (d_{001}) of stevensite and the smectite clay mineral increased by about 4.75 and 0.66 Å respectively, as a result of the interactions between chitosan and clays. Moreover, the shape of these reflexions changed (Fig. 4). These observations indicated that chitosan chains were inserted within the interlayer space of expandable clay minerals. In addition, RH- and BN2-based composites were presumably formed of intercalated/exfoliated and flocculated structures respectively.

Due to the interaction between chitosan and BN2, the shape of the broad IR band linked to the stretching vibrations of O-H bonds (3700–3200 cm^{-1}) was altered, and the stretch bands of OH of kaolinite (3692 cm^{-1}) [20] and illite/

Table 2
Conditions of the planned experiments (experimental design matrix), and measured MB desorption efficiencies of the organoclays studied

Run	X_1	X_2	X_3	I(M)	T(°C)	pH	D (%)	
							BN2-based composite	RH-based composite
1	1.0000	0.0000	0.0000	0.1000	40	6.5	3.06	2.22
2	-1.0000	0.0000	0.0000	0.0000	40	6.5	3.54	3.08
3	0.5000	0.8500	0.0000	0.0750	57	6.5	1.61	1.48
4	-0.5000	-0.8500	0.0000	0.0250	23	6.5	4.83	4.44
5	0.5000	-0.8500	0.0000	0.0750	23	6.5	3.87	2.71
6	-0.5000	0.8500	0.0000	0.0250	57	6.5	1.61	1.97
7	0.5000	0.3000	0.8000	0.0750	46	8.5	1.13	0.25
8	-0.5000	-0.3000	-0.8000	0.0250	34	4.5	6.93	5.01
9	0.5000	-0.3000	-0.8000	0.0750	34	4.5	7.73	6.04
10	0.0000	0.6000	-0.8000	0.0500	52	4.5	8.03	6.38
11	-0.5000	0.3000	0.8000	0.0250	46	8.5	0.97	0.25
12	0.0000	-0.6000	0.8000	0.0500	28	8.5	0.81	0.99
13	0.0000	0.0000	0.0000	0.0500	40	6.5	3.82	3.46
14	0.0000	0.0000	0.0000	0.0500	40	6.5	3.87	3.40
15	0.0000	0.0000	0.0000	0.0500	40	6.5	3.87	3.44

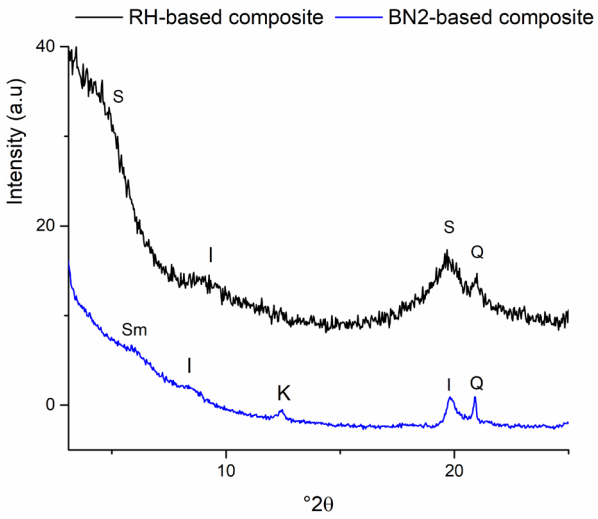

Fig. 4. X-ray diffractograms of the studied chitosan-containing organoclays. S: stevensite; I: illite; K: kaolinite; Sm: smectite clay mineral; Q: quartz.

kaolinite (3625 cm^{-1}) [21] became discernible (Fig. 5a). The alteration of the broad band could be linked to the contribution of the stretching vibrations of O-H (3554 cm^{-1}) and N-H (not well resolved) of chitosan [10]. The manifestation of the bands of kaolinite and illite in the spectrum of the organoclay could be taken as an indication of the absence of significant interactions between hydroxyls of the clay minerals and active moieties of chitosan (amino-groups and hydroxyls). In addition to the latter changes of the IR bands, the frequencies associated to quartz (797 and 779 cm^{-1}) [22] were no longer differentiable (Fig. 5b). It was believed that quartz particles were coated with thick layers of chitosan.

Considering the solid-state NMR spectra given in Fig. 6a, the interaction between chitosan chains and clay minerals particles induced upfield shiftings for tetrahedral (Al^{IV}) and octahedral (Al^{VI}) aluminum ions. The electronic environment of Al^{IV} of stevensite was intensively disturbed ($\Delta\delta$ = 7.7 ppm). The resonance frequency of Si^{4+} (the main cation found in tetrahedral sheets) was almost constant (Fig. 6b). Thus, the close environment of this cation was less affected by the fixation of chitosan. The shielding effect recorded for Al was essentially attributed to the presence of preferential electrostatic interactions between Al^{3+} ions and lone pairs of electrons of –OH and $–NH_2$ groups of chitosan. In the light of these results, it was believed that chitosan was substantially located at free surfaces and edges of the layers of clay minerals, and at the surface of quartz particles.

The microscopic examinations showed that the microstructure of the organoclays consisted of widespread semi-globular grains (Fig. 7). The clay particles, which presented salient edges, almost disappeared and grains with diffuse edges formed. In line with the NMR results, clay minerals were coated with chitosan. The non-clay minerals were also covered with chitosan, but the surface coating seemed to be more pronounced for particles of BN2-based composite. In fact, because of the low quantity of smectite in BN2, only a small amount of chitosan was susceptible to be introduced in the interlamellar space. So, the main remaining portion of the biopolymer should be placed around particles of illite, kaolinite and quartz.

3.2. Adsorption kinetics

The results of the kinetics of MB adsorption on the organoclays showed that about three-fourths of the initial

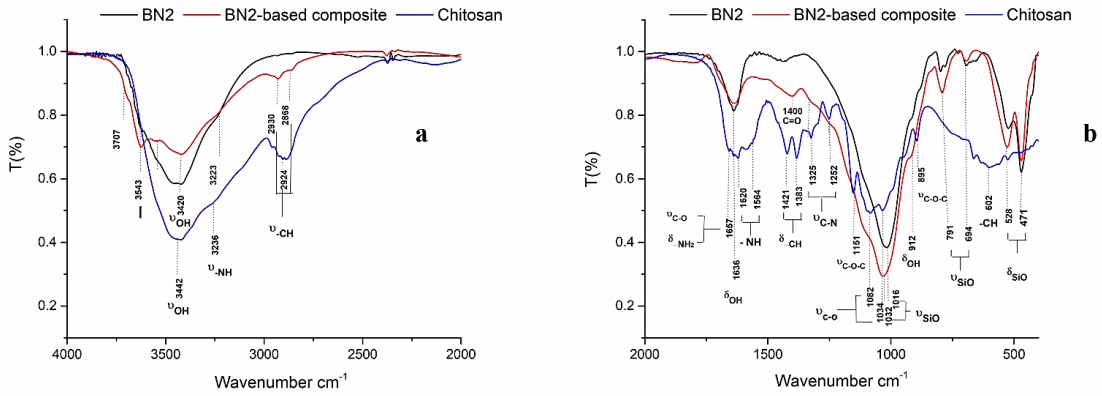

Fig. 5. FT-IR spectra of BN2-based composite and its basic constituents.

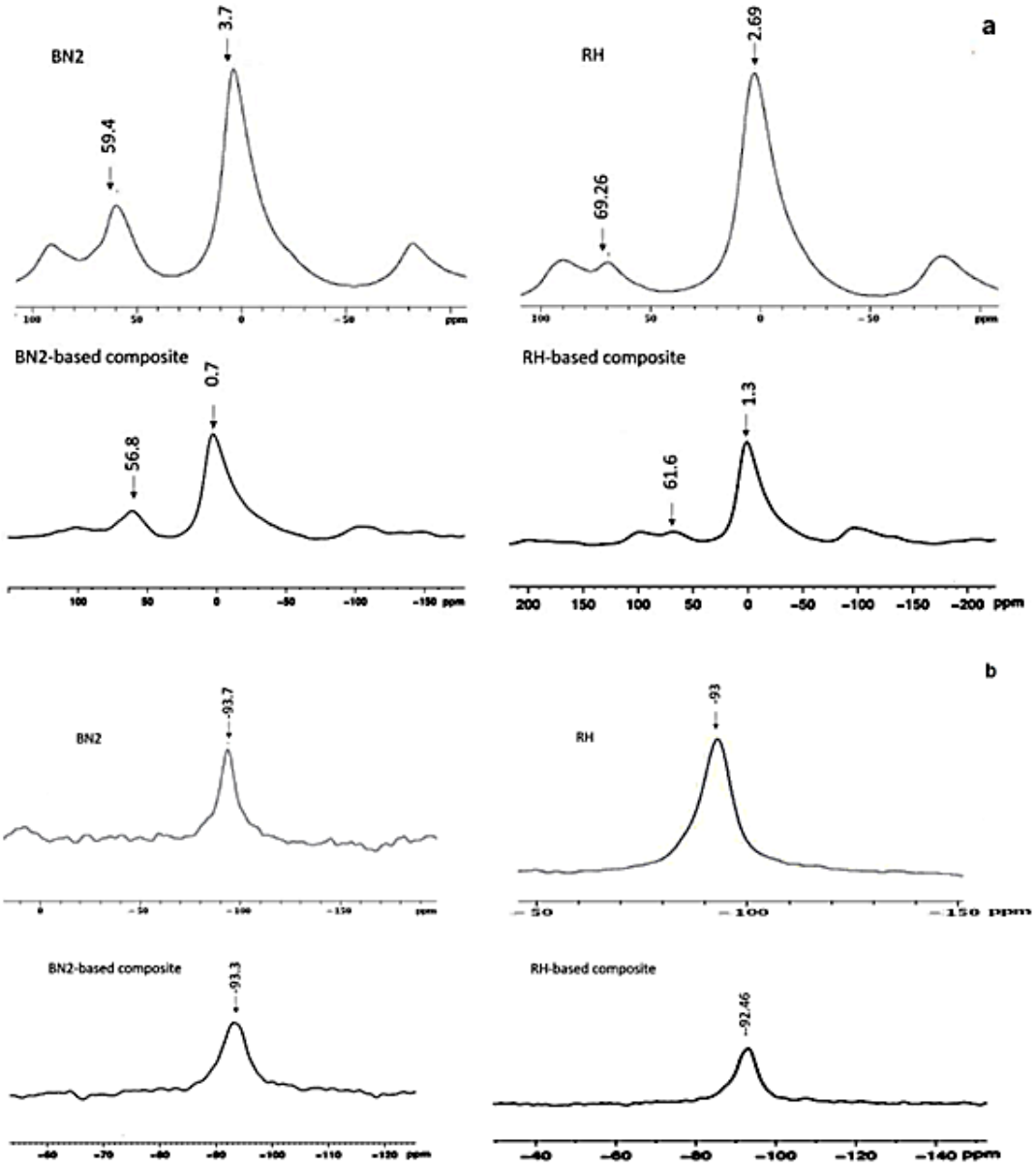

Fig. 6. ^{27}Al (a) and ^{29}Si (b) solid-state NMR spectra of the clays used and their composites.

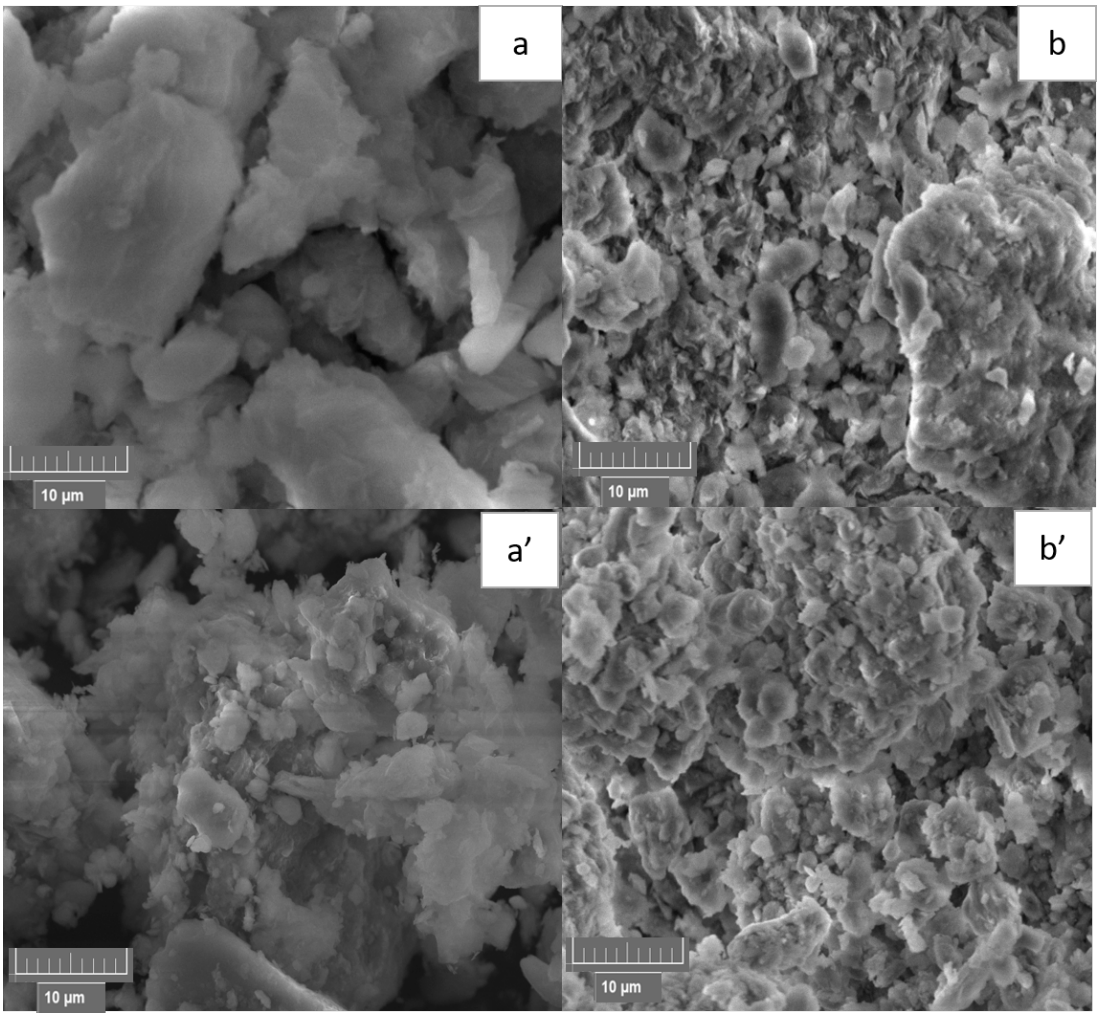

Fig. 7. SEM micrographs of the clays used and their organoclays. (a): RH; (b): RH-based composite; (a'): BN2; (b'): BN2-based composite.

amount of the dye in the solutions was retained by BN2- and RH-based composites in less than 60 and 30 min respectively (Fig. 8). Moreover, the processes of MB adsorption on both organoclays seemed to be endothermic. This effect is quantitatively checked below.

The curves of the kinetics of MB adsorption on BN2-based composite followed perfectly the pseudo-first order kinetic model (Table 3). In contrast, the kinetics curves associated to MB adsorption on RH-based composite well fitted the pseudo-second order equation. In both of the studied cases, the rate constants increased with increasing temperature, and their values varied in the ranges of 0.01–0.04 min^{-1} and 0.5–0.7 g/mmol·min (Table 3).

The activation energies, determined by using the Arrhenius equation ($k = Ae^{-Ea/RT}$, where k: rate constant; E_a: energy of activation; R: gas constant; T: temperature) were found to be 18.81 and 4.43 kJ/mol for BN2- and RH-based composites respectively. Based on these values, it was observed that the barrier energy was considerably low for the exfoliated/intercalated composite, i.e. RH-based composite.

The plots of Bt versus time showed a linear evolution (Fig. 9), but the curves did not pass through the origin, except for the case of MB adsorption on BN2-based composite at 298 K. In view of these results, the process of the kinetics of MB adsorption at 298 K on BN2-based composite was essentially controlled by intraparticle diffusion of MB species. In contrast, the rate limiting steps for the remaining adsorption processes were mainly controlled by film-diffusion [14].

3.3. Adsorption isotherms

The isotherms of MB adsorption on both organoclays showed L-shape (Fig. 10). Such a shape is generally taken as an indication of the presence of micropores together with a high affinity towards adsorbent sites. Referring to Fig. 10, adsorption of MB on both organoclays seemed to be an endothermic process, and the maximum amount retained by RH-based composite was relatively high. Based on the statistical data (R^2, RSME) given in Table 4, the isotherms of BN2-based composite followed better

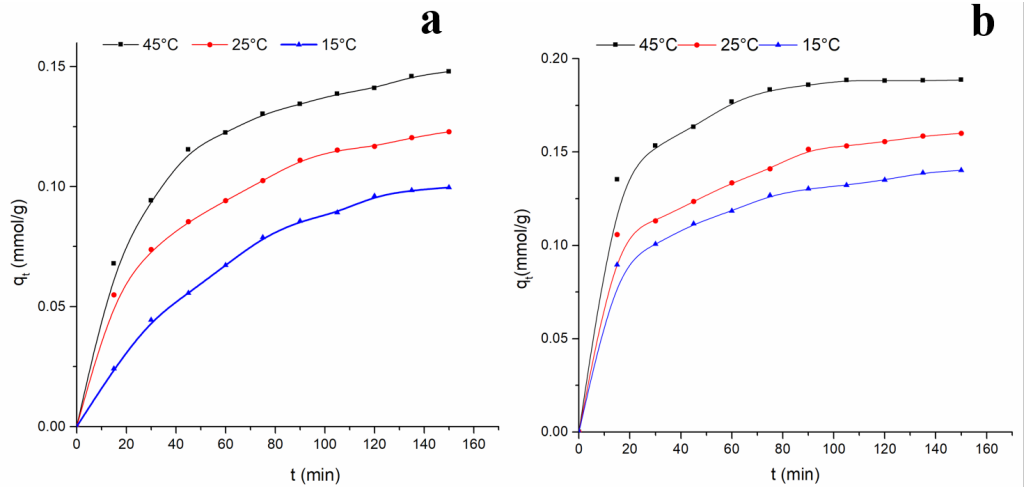

Fig. 8. Curves of the kinetics of MB adsorption on the organoclays studied. (a): BN2-based composite; (b): RH-based composite.

Table 3
Values of the parameters of the pseudo-first and pseudo-second order kinetics models, and the statistical coefficients R^2 and RMCE

	BN2-based composite				RH-based composite	
	T (°C)	15	25	45	15	25	45
	q_{exp} (mmol/g)	0.10	0.12	0.14	0.14	0.16	0.19
Pseudo-first order kinetic model	K_1 (min^{-1})	0.016	0.031	0.036	0.055	0.063	0.074
	R^2	0.99	0.96	0.97	0.81	0.85	0.83
	RMCE	0.001	0.005	0.004	0.008	0.008	0.008
	q_{cal} (mmol/g)	0.11	0.12	0.14	0.131	0.152	0.18
Pseudo-second order kinetic model	K_2 (g/mmol·min)	0.11	0.24	0.25	0.56	0.61	0.67
	R^2	0.98	0.98	0.99	0.95	0.97	0.96
	RMCE	0.007	0.003	0.0014	0.005	0.003	0.004
	q_{cal} (mmol/g)	0.13	0.14	0.17	0.148	0.162	0.19

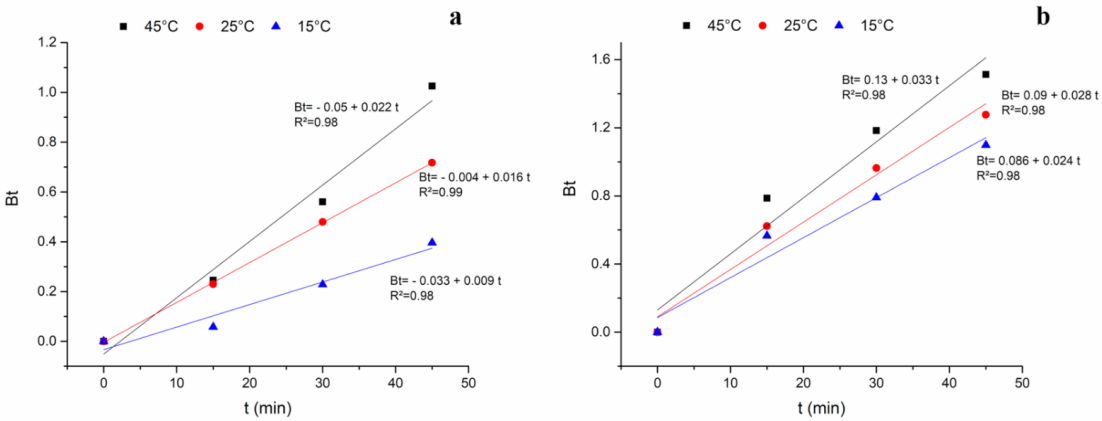

Fig. 9. Plots of the product Bt versus time. (a): BN2-based composite; (b): RH-based composite.

the model of Freundlich. Thus, MB adsorption occurred on heterogeneous sites, and the interactions between the dye species could not be neglected. For RH-based composite, the adequate isotherm model depended on the temperature used: Langmuir's model was well followed at 15 and 25°C, whereas the model of Temkin was more suitable at 45°C. Thus, up to 25°C adsorption took place on homogeneous sites without any interaction between the adsorbed MB species. Moreover, the adsorption heat was considered constant. However, at 45°C lat-

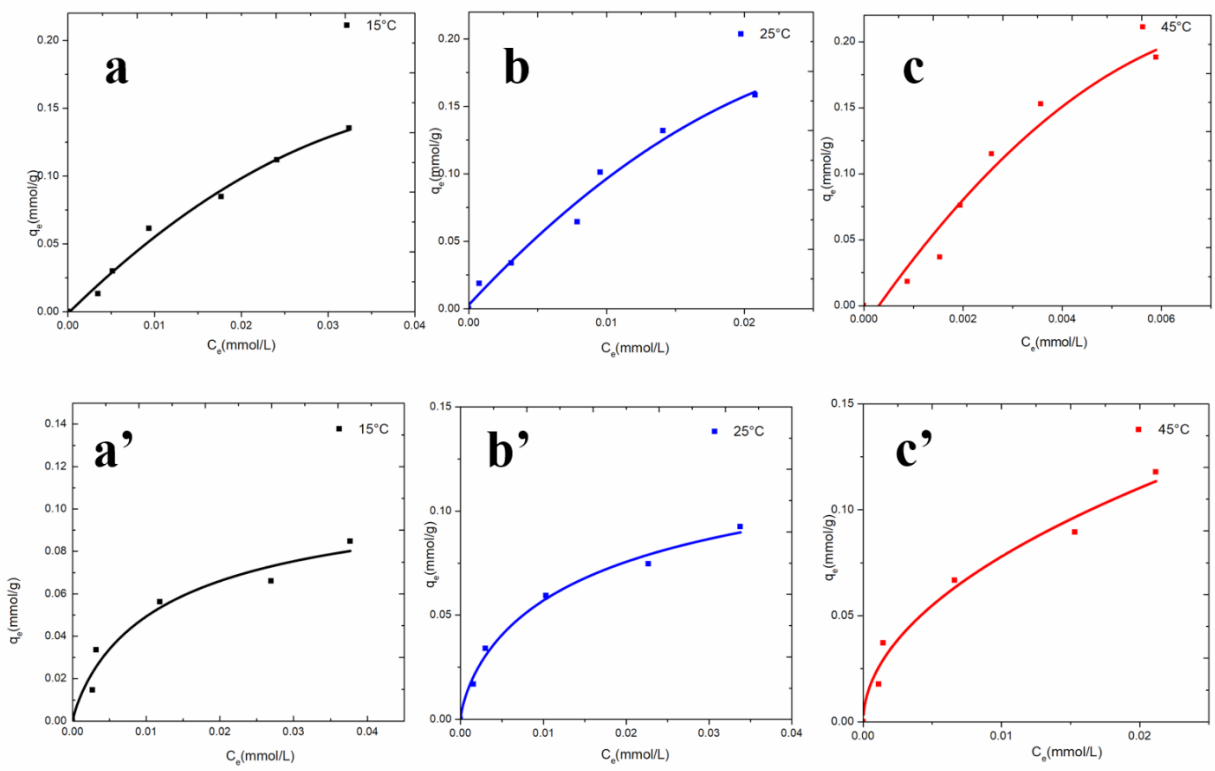

Fig. 10. Isotherms of the adsorption of MB on the organoclays studied. (a, b, c): RH-based composite; (a′, b′, c′): BN2-based composite.

eral repulsive interactions developed between the dye species, and the heat of adsorption decreased linearly with coverage [17].

Taking into consideration the data given in Table 4, the Langmuir maximum uptake increased almost linearly with increasing temperature:

$$q_{e\,max}\,(\text{BN2-based composite ; mmol/g}) = 0.093 + 2.10^{-3}\,T\,(°C)\ (R^2 = 0.86) \quad (6)$$

$$q_{e\,max}\,(\text{RH-based composite; mmol/g}) = 0.076 + 16.10^{-3}\,T\,(°C)\ (R^2 = 0.91) \quad (7)$$

The MB amount retained by RH-based composites was about three times higher than that of BN2-based composites. It seemed that as an intercalated/exfoliated composite, RH-based composite enclosed abundant active sites. The sites involved in the processes of MB retention by both composites are identified hereafter.

Table 4
Values of the parameters of the isotherms models used, and the fitting statistical coefficients R^2 and RMCE

		BN2-based composite			RH-based composite		
	T (°C)	15	25	45	15	25	45
Langmuir model	R^2	0.88	0.94	0.95	0.98	0.97	0.93
	q_m (mmol/g)	0.135	0.14	0.2	0.37	0.43	0.85
	K_L	56.3	73.1	77.2	17	28.25	51.2
	RMCE	0.013	0.01	0.013	0.006	0.01	0.021
Freundlich model	R^2	0.92	0.97	0.97	0.98	0.97	0.91
	K_F (mmol/g·(L/mmol)$^{1/n}$)	0.55	0.54	0.97	2.1	3.11	20.7
	$1/n$	0.54	0.5	0.54	0.8	0.76	0.9
	RMCE	0.011	0.007	0.008	0.007	0.011	0.022
Temkin model	R^2	0.88	0.94	0.93	0.98	0.83	0.96
	K_T(L/mmol)	752	1094	1543	343	1229	11898
	RT/b (mmol/g)	0.027	0.026	0.034	0.053	0.042	0.098
	RMCE	0.013	0.01	0.014	0.007	0.025	0.015

The maximum amount of MB retained by the chitosan-RH composite was as high as the adsorption capacities of some chitosan-clay adsorbents (Table 5). In contrast, the uptake capacity of BN2-based composite was relatively low. Thus, adsorbents, which were composed of chitosan and swelling clay minerals such as montmorillonite and stevensite, were suitable materials for MB retention.

The values of the Gibbs free energy (ΔG°_{T}), the heat (ΔH°_{T}) and the entropy (ΔS°_{T}) of MB adsorption on RH- and BN2-based composites (Table 6) were determined by using the following thermodynamic equations:

Table 5
Maximum amounts of MB retained by some chitosan-clay composites and by the adsorbents studied

Adsorbents	q_m (mg/g)	References
Cross-linked chitosane/bentonite composite	142.86	[9]
Chitosan composite MBC-CH	282.7	[3]
Poly(vinyl alcohol)-sodium alginate-chitosan montmorillonite hydrogel beads	137.2	[23]
Montmorillonite nanosheets (MMTNS) and chitosan (CS) hydrogel	530	[24]
BN2-based composite	64	This study
RH-based composite	272	This study

Table 6
Thermodynamic data related to the MB adsorption on the organoclays studied

	T (K)	ΔG^{o} (kJ/mol)	ΔH^{o} (kJ/mol)	ΔS^{o} (kJ/K·mol)
RH-based composite	288	–32.94	27.43	0.21
	298	–35.34		
	318	–39.29		
BN2- based composite	288	–35.81	7.31	0.15
	298	–37.70		
	318	–40.37		

$$\Delta G^{\circ}_{T} = -RTLnK_e \quad (8)$$

$$LnK_e = -\frac{\Delta H^{\circ}}{RT} + \frac{\Delta S^{\circ}}{R} \quad (9)$$

K_e = 55.5 × $10^3 K_L$ [25]; K_L: Langmuir's constant; R: gas constant (8.31 J $K^{-1}mol^{-1}$); T: temperature (K).

The thermodynamic data showed that MB adsorption on both organoclays took place spontaneously and endothermically. The heat involved in the process of MB retention by RH-based composite was much higher than that related to the MB adsorption on BN2-based composite. This might have a relation with the nature of the sites involved and/or the quantitative retained amount of MB. Based on the values of ΔS°_{T}, the MB adsorption on both composites resulted in an increase of the dispersal energy.

3.4. Desorption efficiency of MB

Based on the values of the statistical parameters given in Table 7, especially the high values of F-ratio and R^2, the adopted quadratic model described perfectly the change of the desorption efficiency of MB versus ionic strength, T and pH. Here are the equations obtained:

$$D(RH-based\ composite) = 3.43 - 0.36X_1 - 0.77X_2 - 3.32X_3 - 0.78X_1^2 - 0.81X_2^2 - 0.005X_3^2 + 0.73X_1X_2 - 0.92X_1X_3 - 1.14X_2X_3 \quad (10)$$

$$D(BN2-based\ composite) = 3.85 - 0.12X_1 - -1.03X_2 - 4.12X_3 - -0.55X_1^2 - 1.017X_2^2 + 1.07X_3^2 + 0.56X_1X_2 - 0.61X_1X_3 - 0.51X_2X_3 \quad (11)$$

Based on the algebraic values of the linear coefficients of both equations, the three factors studied had a negative impact on the release of MB. Moreover, the weights of their effects on the regeneration of MB evolved in the order pH > temperature > ionic strength.

The MB regeneration after different washing cycles was followed under optimum experimental conditions (pH = 4.5, T = 50°C and I = 0.05 M), deduced from Eqns. (10) and (11). The results showed that the release of MB became insignificant after the third washing cycle (Fig. 11). Moreover, MB desorption by RH-based composite was relatively important after the second washing cycle. These findings were related to the nature of the interactions between MB species and adsorbents sites as discussed below.

Table 7
ANOVA results and fitting coefficients (R^2) related to the polynomial models adopted

	Sources of variation	Sum of squares	Degrees of freedom	Mean squares	F-ratio	Signification	R^2
BN2-based composite	Regression	74.2795	9	8.2533	9903.9351	0.0181	0.948
	Residues	4.1003	5	0.8201			
	Total	78.3798	14				
RH-based composite	Regression	48.1959	9	5.3551	5737.6089	0.0247	0.953
	Residues	2.3833	5	0.4767			
	Total	50.5792	14				

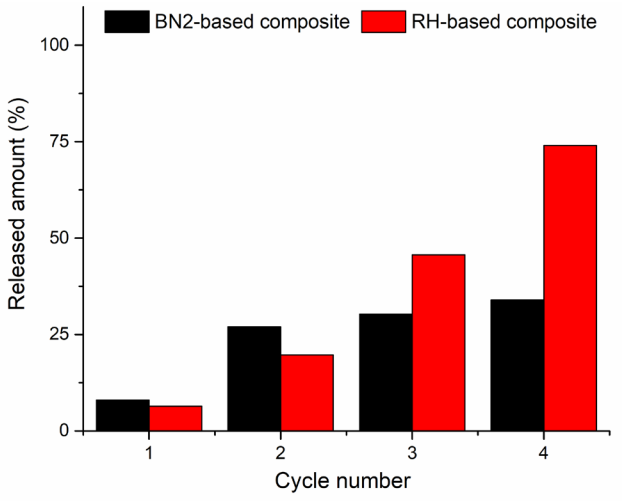

Fig. 11. Changes of the amount of MB released by MB-loaded organoclays versus washing cycle number.

3.5. Mechanisms of MB adsorption

The FT-IR analysis of MB-loaded RH-based composite showed that the bands in the range of 3700–3000 cm^{-1} assignable to the stretching vibrations of OH of water [22], stevensite [26] and chitosan [10] were overlapped (Fig. 12). A partial splitting of the bands was observed after desorption of MB. To have an insight into the adsorption processes behind these facts, the bands in the range of 3700–3000 cm^{-1} were deconvoluted (Fig. 13). Based on the positions of the deconvoluted bands, the clay structural hydroxyls were not involved in the process of the retention of MB species. However, hydroxyls as well as amino-groups of chitosan took part in the process. Taking into consideration the IR bands in the range of 2000–400 cm^{-1} (Fig. 12), it was concluded that: i) MB-loaded organoclay displayed a pronounced hydrophilic behavior. ii) The tetrahedral sheet of stevensite was involved in the retention of MB. This fact was supported by the marked shift of the stretching bands of Si-O (1088 and 1015 cm^{-1}) [27]. iii) The layers of chitosan around quartz particles were partially implicated in MB fixation.

Referring to Fig. 14, MB adsorbed on RH-based composite as MB^+, $(MB^+)_2$ and $(MB^+)_3$. The relative amounts of these species followed the order $MB^+ > (MB^+)_3 > (MB^+)_2$. Considering the maximum adsorption capacity of the composite (up to about 0.8 mmol/g) and the CEC of the organoclay (1.05 meq/g), MB species seemed to be mainly adsorbed by cation exchange, and chitosan was partially involved in the retention process. In the light of these results, it was

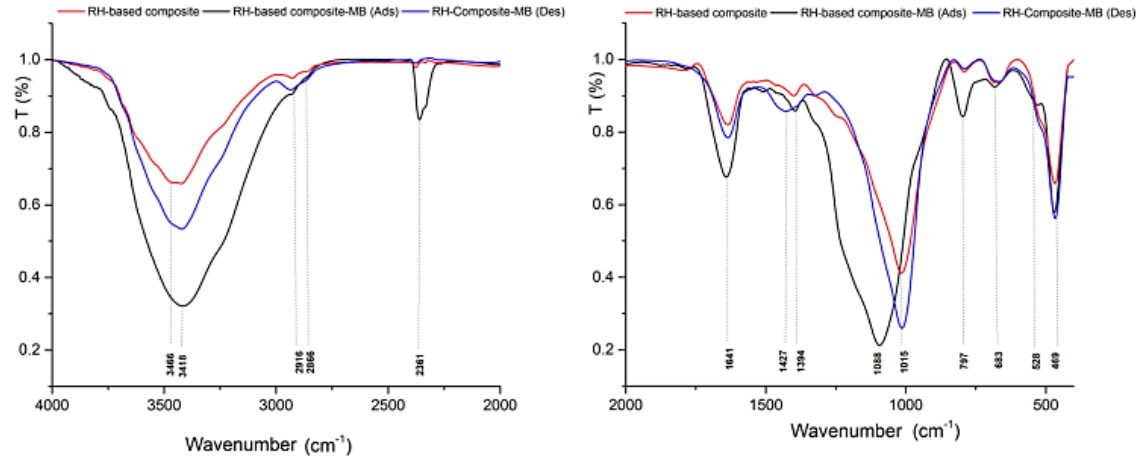

Fig. 12. FT-IR spectra of RH-based composite after adsorption (Ads) and desorption (Des) of MB.

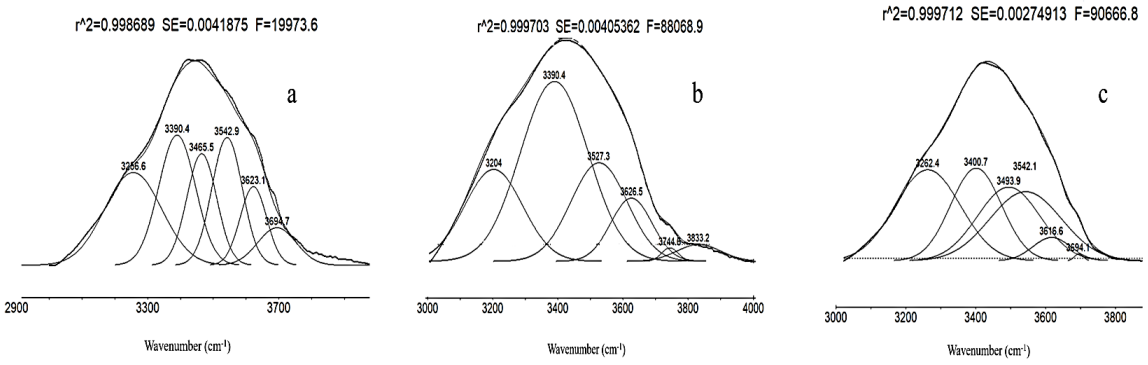

Fig. 13. Deconvoluted bands of the infrared spectra of RH-based composite taken before and after contact with MB (a, b), and after MB desorption (c).

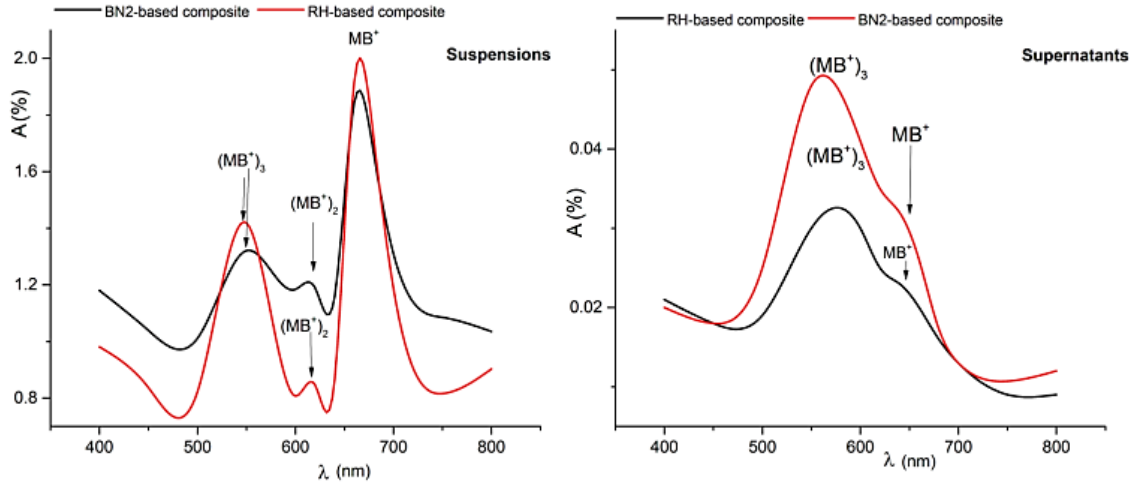

Fig. 14. UV-visible spectra of the suspensions of RH- and BN2-based composites and their corresponding supernatants.

believed that MB^+ ions preferentially adsorbed on external surface sites of the organoclay particles by exchange with Na^+ ions (the starting compensating-charge ions). They were fixed on sites located at surfaces of tetrahedral sheets of stevensite, and did not insert within the interlamellar spaces, which were filled with chains of chitosan. The absence of MB^+ ions within the interlayer was supported by the absence of the UV-visible band at about 653 nm. In addition, it was assumed that MB adsorption on chitosan took place mainly by attractive electrostatic forces established between MB^+ ions and amino-groups of the biopolymer chains, located around the particles. The adsorbed dimer seemed to be formed in the liquid film, found around the particles [28]. In this layer of liquid, the concentration of the monomer should be relatively important. The trimer was believed to form at the surfaces of nanoparticles by molecular stacking [28].

The examination of the FT-IR spectra shown in Fig. 15 indicated that the frequencies related to the bonds of clay minerals (3626, 1034, 922, 528 and 469 cm^{-1}) were not disturbed as a result of MB adsorption on BN2-based composite. In contrast, the shape of the bands assignable to the stretch and deformation of C-H of chitosan (2924, 2858, 1425 and 1398 cm^{-1}) were altered. The deconvolution of the bands in the range of 3700–3000 cm^{-1} revealed that the frequency linked to NH of chitosan (3496 cm^{-1}) experienced a significant change (about 47 cm^{-1}) after MB adsorption. These observations led the deduction that functional moieties of chitosan, particularly amino-groups, were implicated in the retention of MB species. The structural hydroxyls and silica units of tetrahedral sheets of the clay minerals were not directly involved in the adsorption process of MB.

Considering the Langmuir maximum adsorption capacity of BN2-based organoclay (up to about 0.2 mmol/g) and the CEC of the composite (0.39 meq/g), MB species were adsorbed on organoclay particles by a cation exchange mechanism. But, the MB retention by amino-groups of chitosan placed around adsorbent particles should be taken into consideration. In this case, it was believed that the electrostatic interactions between lone pairs of electrons of nitrogen atoms of $–NH_2$ groups of chitosan and MB cations were responsible for MB-chitosan bonding.

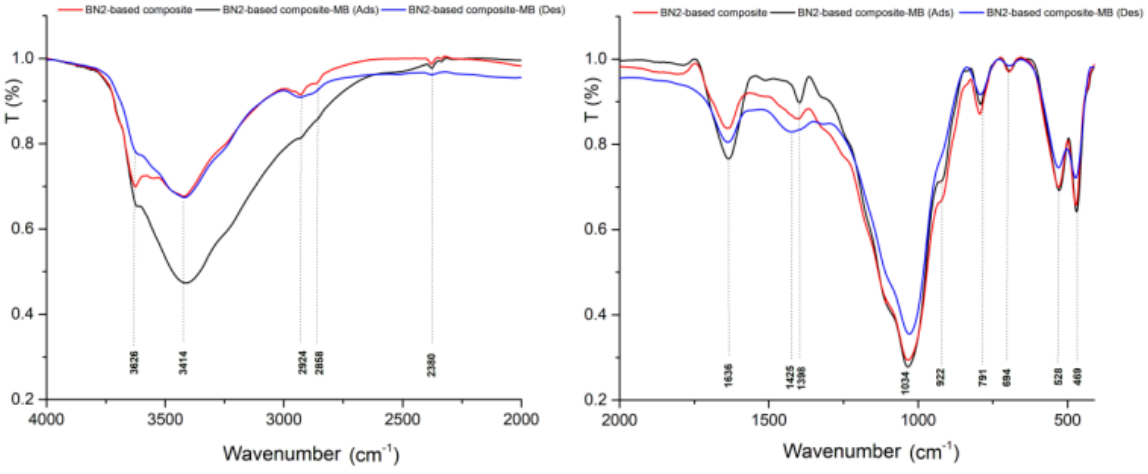

Fig. 15. FT-IR spectra of BN2-based composite after adsorption (Ads) and desorption (Des) of MB.

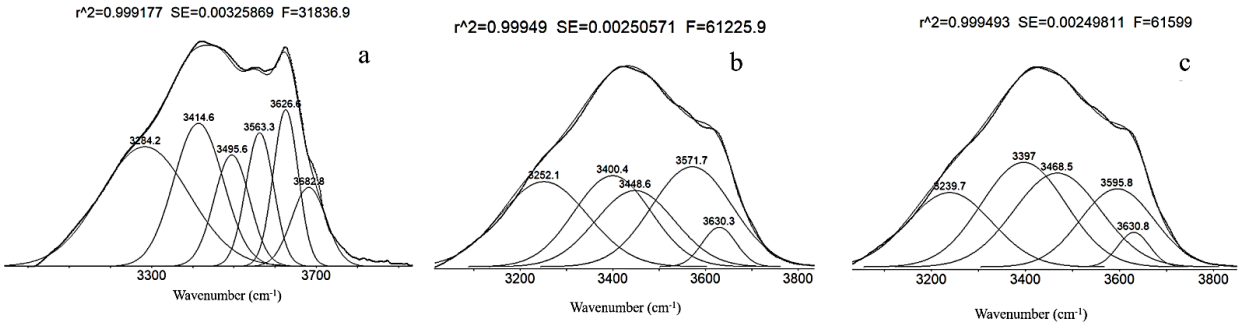

Fig. 16. Deconvoluted bands of the infrared spectra of BN2-based composite taken before and after contact with MB (a, b), and after MB desorption (c).

Based on the UV-visible spectra shown in Fig. 14, MB adsorbed as MB^+, $(MB^+)_2$ and $(MB^+)_3$. The relative abundance was similar to that reported for RH-based composite, and the dimerization and trimerization of MB possibly occurred as proposed before.

4. Conclusion

The results of this study allowed the following conclusions: i) Chitosan was inserted into interlamellar spaces of stevensite, which was the main clay mineral of RH-based composite. In such a condition, the intercalated/exfoliated structure was formed. In contrast, for kaolinitic-illitic based composite, chitosan was mainly placed around particles, and accordingly tactoids were formed. ii) The kinetics data of MB adsorption on BN2- and RH-based organoclays were described by the pseudo-first and pseudo-second order kinetics models respectively, and MB diffusion across the liquid film around particles was the main rate-limiting step. The rate constants were in the ranges of 0.01–0.04 min^{-1} and 0.5–0.7 g/mmol·min respectively, and the energies of activation were found to be 18.81 and 4.43 kJ/mol. iii) The adsorption isotherms of BN2-based composite fitted better the model of Freundlich, whereas those related to RH-based composite followed perfectly the models of Langmuir and Temkin, depending on the temperature used. The MB maximum quantities retained by both organoclays increased with increasing temperature, and the uptakes at 318 K were of 64 and 272 mg/g for BN2- and RH-based composites. MB adsorption on both organoclays occurred spontaneously. The Gibbs free energies varied between –41 and –32 kJ/mol, and the heats were of 27.43 and 7.31 kJ/mol for RH- and BN2-composites respectively. iv) The weights of the effects of pH, ionic strength and temperature on the desorption efficiency of MB received a good evaluation from the quadratic models obtained. Based on these models, the increase of the values of the factors had an adverse effect on MB desorption, and their weights followed the order pH > temperature > ionic strength. v) MB species were retained by both organoclays as MB^+, $(MB^+)_2$ and $(MB^+)_3$. The formation of the dimer and trimer was presumably due to the build-up of MB^+ ions in the vicinity of the surfaces of particles, and to the high surface area of the nano-sized particles of the organoclays. MB cations were adsorbed on external surface sites of the organoclay particles by cation exchange. Also, they were attached to chitosan chains by attractive electrostatic forces, which mainly involved the amino-groups of the biopolymer.

Acknowledgement

The authors are grateful to CNRST for its financial support (grant no. PPR/26/2015).

References

[1] H. He, L. Ma, J. Zhu, R.L. Frost, B.K.G. Theng, F. Bergaya, Synthesis of organoclays: A critical review and some unresolved issues: A critical review and some unresolved issues, Appl. Clay Sci., 100 (2014) 22–28.
[2] L.B. de Paiva, A.R. Morales, F.R.V. Díaz, Organoclays: Properties, preparation and applications, Appl. Clay Sci., 42 (2008) 8–24.
[3] M. Auta, B.H. Hameed, Chitosan-clay composite as highly effective and low-cost adsorbent for batch and fixed-bed adsorption of methylene blue, Chem. Eng. J., 237 (2014) 352–361.
[4] Y. Xu, X. Ren, M.A. Hanna, Chitosan/clay nanocomposite film preparation and characterization, J. Appl. Polym. Sci., 99 (2005) 1684–1691.
[5] Y.S. Han, S.H Lee, K.H. Choi, I. Park, Preparation and characterization of chitosan – clay nanocomposites with antimicrobial activity, J. Phys. Chem. Solids, 71 (2010) 464–467.
[6] K. Lewandowska, A. Sionkowska, B. Kaczmarek, G. Furtos, Characterization of chitosan composites with various clays, Int. J. Biol. Macromol., 65 (2014) 534–541.
[7] M. Rafatullah, O. Sulaiman, R. Hashim, A. Ahmad, Adsorption of methylene blue on low-cost adsorbents: A review, J. Hazard. Mater., 177 (2010) 70–80.
[8] G. Stassinos, Methylene blue. The Maryland Poison Center's, University of Marylandand School of Pharmacy, ToxTidbits (2015).
[9] Y. Bulut, H. Karaer, Adsorption of methylene blue from aqueous solution by crosslinked chitosan/bentonite composite, J. Dispers. Sci. Technol., 36 (2015) 61–67.
[10] S. Ba, A. Alagui, M. Hajjaji, Retention and release of hexavalent and trivalent chromium by chitosan, olive stone activated carbon, and their blend, Environ. Sci. Pollut. Res., 25 (2018) 19585–19604.
[11] J. Brugnerotto, J. Lizardi, F.M. Goycoolea, W. Arguelles-Monal, J. Desbrières, M. Rinaudo, An infrared investigation in relation with chitin and chitosan characterization, Polymer, 42 (2001) 3569–3580.
[12] A. Tolaimate, J. Desbrières, M. Rhazi, A. Alagui, Contribution to the preparation of chitins and chitosans with controlled physico-chemical properties, Polymer, 44 (2003) 7939–7952.

[13] M.N.V.R Kumar, A review of chitin and chitosan applications, React. Funct. Polym., 46 (2000) 1–27.
[14] R.M.C. Viegas, M. Campinas, H. Costa, M.J. Rosa, How do the HSDM and Boyd's model compare for estimating intraparticle diffusion coefficients in adsorption processes, Adsorption, 20 (2014) 737–746.
[15] I. Langmuir, The adsorption of gases on plane surfaces of glass, mica and platinum, J. Am. Chem. Soc., 40 (1918) 1361–1403.
[16] H. Freundlich, Über die Adsorption in Lösungen, Zeitschrift-Für Phys. Chemie, 57 (1907) 385–470.
[17] M.J. Temkin, V. Pyzhev, Recent modifications to Langmuir isotherms, Acta Physiochim USSR, 12 (1940) 217.
[18] S.L.C. Ferreira, N.L. Walter, C.M. Quintella, B.B. Neto, J.M. Bosque-sendra, Doehlert matrix: a chemometric tool for analytical chemistry - review, Talanta, 63 (2004) 1061–1067.
[19] D. Mathieu, R. Phan Ta Luu, Software NEMROD, Université d'Aix-Marseille III, France (1980).
[20] J. Madejova, FTIR techniques in clay minerals studies: A review, Vib. Spectrosc., 31 (2003) 1–10.
[21] G.M. Ndzana, L. Huang, J.B. Wang, Z.Y. Zhang, Characteristics of clay minerals in soil particles from an argillic horizon of Alfisol in central China, Appl. Clay Sci., 151 (2018) 148–156.
[22] K. El Hafid, M. Hajjaji, Effects of the experimental factors on the microstructure and the properties of cured alkali-activated heated clay, Appl. Clay Sci., 116–117 (2015) 202–210.
[23] W. Wang, Y. Zhao, H. Bai, T. Zhang, V. Ibarra-Galvan, S. Song, Methylene blue removal from water using the hydrogel beads of poly(vinyl alcohol)-sodium alginate-chitosan-montmorillonite, Carbohydr. Polym., 198 (2018) 518–528.
[24] S. Kang, Y. Zhao, W. Wang, T. Zhang, T. Chen, H. Yi, F. Rao, S. Song, Removal of methylene blue from water with montmorillonite nanosheets/chitosan hydrogels as adsorbent, Appl. Surf. Sci., 448 (2018) 203–211.
[25] H.N. Tran, S.J. You, A. Hosseini-Bandegharaei, H.P. Chao, Mistakes and inconsistencies regarding adsorption of contaminants from aqueous solutions: A critical review, Water Res., 120 (2017) 88–116.
[26] M. Hajjaji, A. Beraa, Y. Coppel, R. Laurent, A.M. Caminade, Adsorption capacity of sodic-and dendrimers-modified stevensite, Clay Miner., 53(2018) 1–20.
[27] M.A. Soleimani, R. Naghizadeh, A.R. Mirhabibi, F. Golestanifard, Effect of calcination temperature of the kaolin and molar Na_2O/SiO_2 activator ratio on physical and microstructural properties of metakaolin based geopolymers, Iran. J. Mater. Sci. Eng., 9 (2012) 43–51.
[28] J. Cenens, R.A. Schoonheydt, Visible spectroscopy of methylene blue on hectorite, laponite B, and barasym in aqueous suspension, Clays Clay Miner., 36 (1988) 214–224.